Chinese Chemical Letters 33 (2022) 1263–1266

Contents lists available at ScienceDirect

Chinese Chemical Letters

journal homepage: www.elsevier.com/locate/cclet

Crystallinity engineering of Au nanoparticles on graphene for *in situ* SERS monitoring of Fenton-like reaction

Danni Guo[a,b], Lixia Zhao[a,*], Hui Zhang[a,c,*]

[a] State Key Laboratory of Environmental Chemistry and Eco-toxicology, Research Center for Eco-environmental Sciences, Chinese Academy of Sciences, Beijing 100085, China
[b] College of Resources and Environment, University of Chinese Academy of Sciences, Beijing 100049, China
[c] State Key Laboratory of Water Environment Simulation, School of Environment, Beijing Normal University, Beijing 100875, China

ARTICLE INFO

Article history:
Received 6 May 2021
Revised 4 June 2021
Accepted 22 July 2021
Available online 31 July 2021

Keywords:
Au nanoparticle
Crystallinity engineering
Fenton-like reaction
SERS monitoring
Environmental remediation

ABSTRACT

Fabrication of multifunctional nanoplatform to *in situ* monitor Fenton reaction is of vital importance to probe the underlying reaction process and design high-performance catalyst. Herein, a hybrid catalyst comprising of single-crystalline Au nanoparticles (SC Au NPs) on reduced graphene oxide (RGO) sheet was prepared, which not only exhibited an excellent $^1O_2$ mediated Fenton-like catalytic activity in promoting rhodamine 6G (R6G) degradation by activating H_2O_2, but also displayed a sensitive surface-enhanced Raman spectroscopy (SERS) detection performance to R6G with a linear response range from 1.0×10^{-8} mol/L to 1.0×10^{-5} mol/L thus providing a powerful and versatile nanoplatform for *in situ* SERS monitoring Fenton-like catalytic reaction. The integration of catalytic and SERS activities into a single nanostructure are expected to provide great potentials for practical applications in environmental catalysis.

Advanced oxidation processes (AOPs) have been regarding as promising and robust technologies in both scientific and industrial fields to decontaminate biorecalcitrant wastewater containing textile dyes, antibiotics, pesticides and landfill leachate [1–3]. As one of the most efficient AOPs, Fenton reaction could produce highly reactive hydroxyl radicals ($^{\bullet}OH$, $E^0(^{\bullet}OH/H_2O) = 2.8$ V *vs.* NHE) from H_2O_2/Fe^{2+} system to oxidize refractory organic contaminants [4,5]. However, several inherent drawbacks of the classical Fenton process, *e.g.*, narrow pH working range and the significant iron sludge formation, limit their further scale-up applications [6]. Heterogeneous Fenton catalysts, such as iron oxides, iron-immobilized clays, supported gold (Au) nanoparticles and bifunctional metal structures, have been subsequently developed to address these disadvantages [7–9]. Understanding how the catalytic reactions occur on the surface of the catalyst is thus essential to design potential energetic catalysts, which requires us to probe the Fenton-like reaction *in situ* with high sensitivity.

Numerous strategies such as liquid/gas chromatography and mass spectrometry have been applied to investigate catalytic activity and reaction kinetics of Fenton catalysts [10,11]. These analytical methods are sensitive for product identification, but neither could provide reaction information on the catalyst surface nor monitor the reaction process in real time [12]. Therefore, the detailed characterization of Fenton-like reaction process is of particular interest. As a molecular surface-specific spectroscopic technique, surface-enhanced Raman spectroscopy (SERS) based on noble metal nanostructures (*e.g.*, Au, Ag) has contributed to various fields due to its ultrasensitive, non-destructive and fingerprint-like characteristics [13]. SERS shows significant potential for label-free monitoring heterogeneous catalytic reaction, which refers to fabricate bifunctional platforms with both plasmonic property and catalytic activity. For example, integrating SERS-active nanoparticle (Au) with catalytic nanoparticles (Pt or Pd) provide opportunities for *in situ* monitoring of reactions catalyzed by Pt or Pd *via* SERS [14]. The combination of plasmonic metal with semiconductors represents an attractive approach to *in situ* detect the photocatalytic reaction by SERS [15]. However, there are few reports about *in situ* monitoring Fenton-like reactions *via* SERS.

The challenge of developing platform with both Fenton catalytic and SERS activity lies in that the presence of Fenton catalysts usually induces the intense suppression of plasmonic field of metal nanostructures [16]. Although Au nanoparticles (NPs) possess both catalytic and SERS activity, the size-dependent physicochemical properties make them either provide SERS enhancement at > 20 nm or exhibit catalytic activity at < 10 nm [17]. Anchoring Au NPs on a support could endow them with Fenton catalytic activity [18]. However, this yields insufficient plasmonic activity for SERS detection. The central dilemma is therefore integrating

* Corresponding authors.
E-mail addresses: zlx@rcees.ac.cn (L. Zhao), zhanghui@bnu.edu.cn (H. Zhang).

https://doi.org/10.1016/j.cclet.2021.07.051
1001-8417/

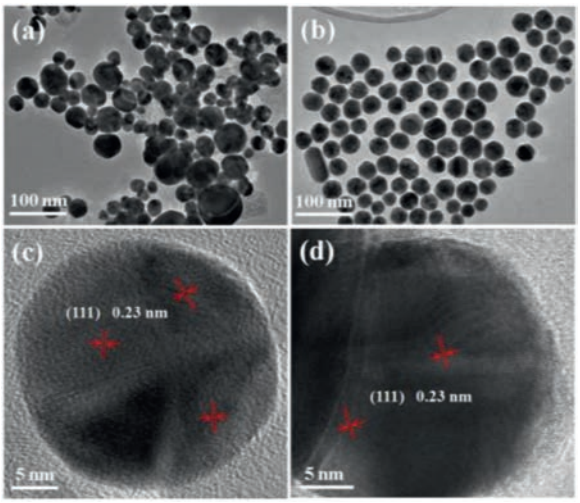

Fig. 1. TEM and HRTEM images of (a, c) MT Au NPs/RGO and (b, d) SC Au NPs/ RGO hybrids.

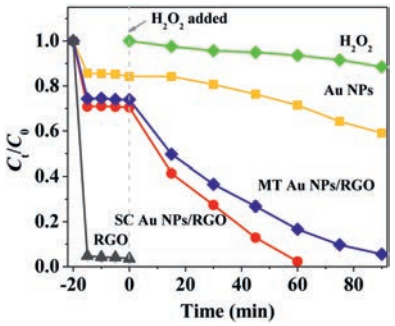

Fig. 2. Degradation curves of R6G in different catalysts/H_2O_2 systems. Reaction conditions: [R6G] = 10^{-5} mol/L, [H_2O_2] = 0.2 mol/L, pH 7.6, [Au NPs/RGO] = 53 mg/L, [Au NPs] = 47 mg/L, [RGO] = 0.75 mg/L. C_t is the R6G concentration at reaction time t, and C_0 is the initial concentration. t = 0 represents that H_2O_2 was added into the catalyst suspensions.

both functions into a single unit [19]. Fortunately, two-dimensional graphene provides a unique platform to mediate optical and catalytic properties of Au NPs, which significantly enhance SERS activity or peroxidase-like catalytic activity [20]. However, the Fenton catalytic activity of Au NPs/graphene has not yet been explored. Considering the electronic coupling between Au NPs and graphene, it is anticipated that crystallinity engineering Au NPs on graphene would enable them to simultaneously possess Fenton catalytic activity and strong plasmonic field at the catalyst surface. Inspired by crystallinity engineering, we report herein a facile approach to achieve controllable growth of single-crystalline (SC) Au NPs on reduced graphene oxide (RGO) to endow SERS active Au NPs/RGO hybrids with Fenton catalytic activity. Rhodamine 6G (R6G) dye was selected as target molecule to investigate SERS sensitivity and Fenton-like catalytic activity of Au NPs/RGO substrate due to its well-established spectra features.

The homogeneity is a prerequisite for a reproducible and reliable SERS substrate. To achieve homogenous growth of Au NPs on graphene sheets, a sonolytic followed by hydrothermal approach was developed to synthesize Au NPs/RGO hybrids. Fig. 1 shows typical transmission electron microscopy (TEM) images of the as-prepared Au NPs/RGO hybrids. Without sonolytic pretreatment, irregular Au NPs with a broad size distribution (33.3 ± 11.2 nm, Fig. S1 in Supporting information) was observed on RGO surface (Fig. 1a), while the sonolytic pretreatment resulted in a uniform Au NPs deposition throughout the graphene sheet with a narrow size distribution (33.0 ± 4.0 nm) (Fig. 1b). The high-resolution TEM images of both Au NPs/RGO hybrids (Figs. 1c and d) displays that Au NPs were mainly composed of (111) planes with a lattice fringe of 2.3 Å, which could be indexed to face-centered cubic (fcc) crystal structure of Au crystal [21]. Interestingly, Au NPs in both hybrids exhibited distinct twin boundaries. The majority of Au nanocrystals were multiply twinned (MT) for the samples prepared without sonolytic pretreatment, while sonolytic pretreatment resulted in a low twinning density and yielded a single-crystalline (SC) structure of Au nanocrystals. The selected area electron diffraction patterns (SAED) further confirmed the crystallographic structure of Au nanocrystals. The ring pattern in Fig. S2a (Supporting information) clearly indicates the polycrystalline nature of Au NPs, while the lattice pattern in Fig. S2b (Supporting information) demonstrates a SC structure of Au nanocrystals. These results highlight the significant role of sonolytic treatment in achieving Au nuclei formation on GO sheet and then facilitating the nanocrystal growth during the hydrothermal process [22]. The homogenous growth of Au NPs on RGO may provide higher density hotspots to enhance SERS signal.

The formation of Au NPs/RGO hybrids was further confirmed by the typical signals of Au $4f_{7/2}$ and $4f_{5/2}$ states (Fig. S3a in Supporting information) [23]. In addition, compared with the initial GO, the peaks of oxy-functional groups in Au NPs/RGO hybrids decreased obviously, indicating the reduction of GO during the hydrothermal process (Fig. S3b in Supporting information) [22]. X-ray diffraction (XRD) patterns of Au NPs reveals typical diffraction peaks indexed to (111), (200), (220) and (311) plans of Au fcc crystal structure, indicating the crystalline character of Au NPs grown on RGO sheet (Fig. S3c in Supporting information) [21]. Fig. S3d (Supporting information) displays UV-vis spectra of the prepared Au NPs/RGO hybrids. An absorption peak located at 535 nm was clearly observed in both Au NPs/RGO hybrids, which could be attributed to the characteristic surface plasmon resonance (SPR) absorption of Au NPs. Compared to MT Au NPs/RGO, the SPR absorption band of SC Au NPs/RGO become narrower, indicating a uniform size distribution of Au NPs in the hybrids, as confirmed by TEM observations.

The Fenton-like catalytic activity of the prepared Au NPs/RGO hybrids was evaluated by degrading R6G in the presence of H_2O_2 (Fig. 2). Prior to the addition of H_2O_2, about 30% of R6G molecules were adsorbed on Au NPs/RGO hybrids surface when reaching the adsorption equilibrium state. H_2O_2 alone induced little R6G degradation, suggesting that the activation of H_2O_2 could not occur without solid catalysts. Less than 40% of R6G was degraded in 90 min in pristine Au NPs system, indicating Au NPs possessed a low ability to active H_2O_2. Meanwhile, the pristine RGO displayed significant adsorption capacity toward R6G molecules, while it could hardly activate H_2O_2 to degrade R6G (Fig. S4 in Supporting information). Impressively, a sharp drop of R6G concentration occurs over Au NPs/RGO hybrids after the introduction of H_2O_2. Almost 100% decomposition of R6G was achieved within 60 min for SC Au NPs/RGO catalysts and about 85% decomposition was observed for MT Au NPs/RGO catalysts under the same conditions. These results indicated that the synergetic coupling effect that occurred at the interface between poorly active Au NPs and inert RGO is essential in activating Fenton-like reaction. Notably, SC Au NPs/RGO hybrids exhibited a superior Fenton-like catalytic activity to their counterpart MT Au NPs/RGO hybrids. Due to the equivalent dosages of Au NPs/RGO hybrids, the different Fenton-like catalytic performances between two hybrids can merely be ascribed to crystallinity discrepancy of the anchored Au NPs. The high crystallinity character and uniform size distribution of SC Au NPs on RGO sheet may induce more active sites to promote the Fenton-like reaction.

The multifunctional properties of Au NPs/RGO hybrids were further demonstrated by evaluating their SERS performance. The

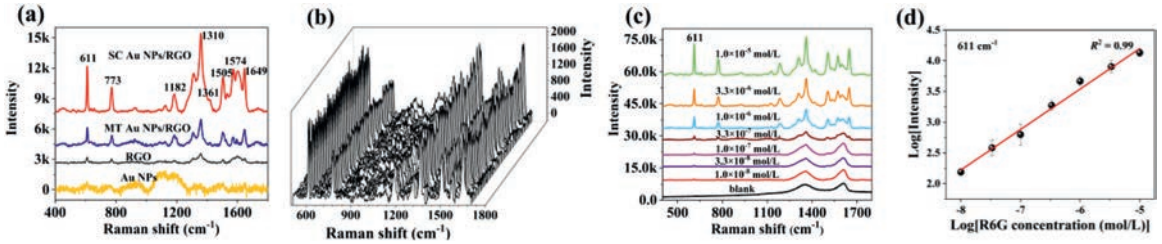

Fig. 3. (a) Raman spectra of R6G (1.0×10^{-6} mol/L) obtained from different substrates. (b) SERS spectra of R6G collected at 50 points over a 5 μm × 10 μm area with a step size of 1 μm from SC Au NPs/RGO substrate. (c) SERS spectra of R6G on SC Au NPs/RGO substrate with concentrations ranging from 1.0×10^{-8} mol/L to 1.0×10^{-5} mol/L. (d) The relationship between R6G concentration and SRES peak intensity at 611 cm^{-1} band.

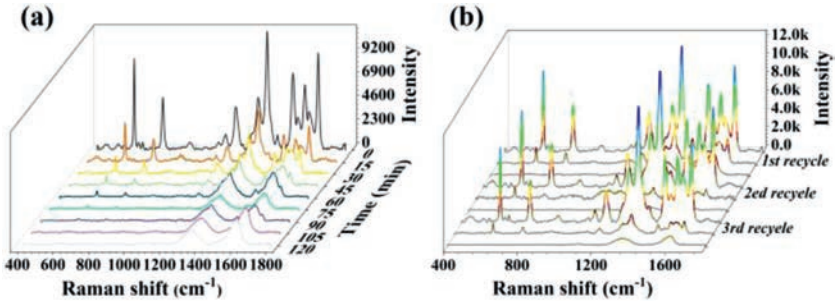

Fig. 4. (a) SERS spectra of R6G on SC Au NPs/RGO substrate at different time intervals after the addition of H_2O_2. (b) Recycle experiment tests of SC Au NPs/RGO substrate for monitoring R6G catalytic degradation process. The initial concentration of R6G is 3.3×10^{-6} mol/L.

top-view and cross-sectional SEM images of the SC Au NPs/RGO substrate displayed that the stacked RGO layers formed a uniform membrane with an approximate thickness of 0.65 μm (Fig. S5 in Supporting information), which indicates that it may provide high uniformity to meet the reliability of SERS quantitative analysis. Fig. 3a represents the characteristic Raman bands of R6G molecule, which could be assigned to vibration modes of C–C–C ring, C–H, and aromatic C–C groups [24]. Interestingly, SC Au NPs/RGO substrate exhibited a superior SERS intensity compared with other substrates. The calculated enhancement factor (EF) of SC Au NPs/RGO substrate at 611 cm^{-1} band is 1.9×10^5, which is about 2.5 times and 8.6 times higher than that of MT Au NPs/RGO substrate ($EF = 7.7 \times 10^4$) and RGO substrate ($EF = 2.2 \times 10^4$), respectively. The significant SERS performance of SC Au NPs/RGO substrate is mostly attributed to the homogeneous distribution of Au NPs on RGO sheet, which may provide appropriate interparticle gap and thus produce higher density of hot spots. The SERS signal reproducibility of SC Au NPs/RGO substrate was further investigated (Fig. 3b). The relative standard deviations (RSDs) for the character peaks at 611 and 773 cm^{-1} were estimated to be 8.4% and 9.7%, respectively (Fig. S6 in Supporting information). The excellent reproducibility of the SC Au NPs/RGO substrate makes it meet well with the requirements of quantitative analysis of target molecules.

The SERS sensitivity of SC Au NPs/RGO substrate was evaluated by R6G molecules with various concentrations. As shown in Fig. 3c, a distinct signal is observed even at a R6G concentration of 1.0×10^{-8} mol/L, indicating the high SERS sensitivity of SC Au NPs/RGO substrate. With increasing R6G concentration, the intensity of SERS signals gradually enhanced. Fig. 3d further presents the relationship between the logarithmic R6G concentration and logarithmic SERS intensity at 611 cm^{-1} band. A good linear dependence was observed in a R6G concentration range from 1.0×10^{-8} mol/L to 1.0×10^{-5} mol/L with R^2 as 0.99. These results demonstrate that SC Au NPs/RGO substrate could be sensitive and applicable for SERS detection.

Combined with the excellent Fenton-like activity and high SERS sensitivity, SC Au NPs/RGO substrate exhibits great potentials to *in situ* SERS monitoring of Fenton-like catalytic reaction. Fig. 4a shows the SERS monitoring of R6G degradation by H_2O_2 activated by SC Au NPs/RGO hybrids. It displayed that the SERS intensities of R6G characteristic peaks decreased gradually with prolonging the reaction time after H_2O_2 addition, indicating the progressive degradation of R6G molecules. The characteristic Raman bands of R6G molecule at 611 cm^{-1} (C–C–C ring vibration), 773 cm^{-1} (C–H vibration) and 1182 cm^{-1} (C–H vibration) nearly disappeared within 90 min, which suggested that R6G molecules were almost completely degraded [24]. According to the time-dependent Raman intensity of R6G, the kinetic parameters of the degradation process were determined. Fig. S7 (Supporting information) plotted the logarithm of the Raman intensities *versus* the reaction time. A good linear relationship suggests that the degradation of R6G molecules by H_2O_2 follows pseudo-first-order kinetics with the degradation rate constants of 0.0412 min^{-1}, 0.0397 min^{-1} and 0.0413 min^{-1} at 611 cm^{-1}, 773 cm^{-1} and 1182 cm^{-1}, respectively. The similar degradation rate constants at different characteristic Raman bands suggest an excellent performance of SERS in detecting Fenton-like reactions.

The recyclability of SC Au NPs/RGO substrate was further investigated by conducting R6G degradation process over three cycles (Fig. 4b). After incubated in H_2O_2 solution for 90 min, SC Au NPs/RGO substrate was almost completely reversed to their initial state. The Fenton catalytic activity and SERS sensitivity do not significantly decrease during the recycle experiments. The typical SEM image of SC Au NPs/RGO substrate after three cycles exhibited no distinct change of the substrate (Fig. S8 in Supporting information). These results illustrate that the developed SC Au NPs/RGO substrate possesses good reusability and can be recycled for *in situ* SERS monitoring of Fenton-like reaction.

To investigate the underlying Fenton-like catalytic process, the generated reactive oxygen species (ROS) was identified by electron spin resonance (ESR) spectra using 5,5-dimethyl-1-pyrroline *N*-oxide (DMPO) and 2,2,6,6-tetramethyl-4-piperidinol (TEMP) as the trapping agent. A typical quadruple peak signal of DMPO-$HO^{\bullet}$ adduct (1:2:2:1) was observed in Au NPs/H_2O_2 and MT Au NPs/RGO/H_2O_2 systems (Fig. 5a), which are expected in

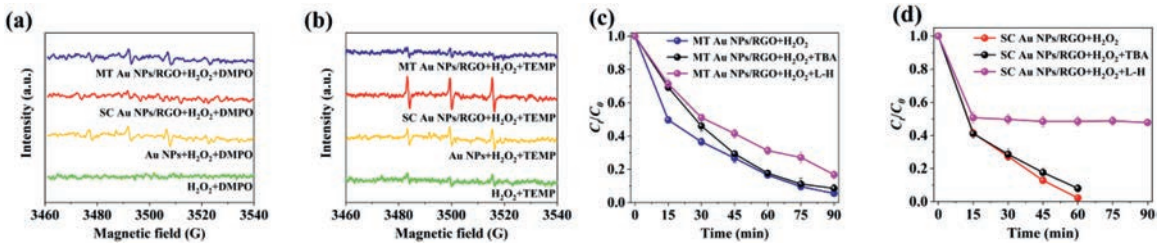

Fig. 5. ESR spectra of (a) DMPO and (b) TEMP spin-trapping adducts in different reaction systems. R6G Degradation curves in (c) MT Au NPs/RGO and (d) SC Au NPs/RGO suspensions with the addition of radical scavengers. *Tert*-butyl alcohol (2 mmol/L) and L-histidine (1 mmol/L) were used to quench ·OH and for $^1O_2$, respectively.

classic Fenton-like reaction generated through the Haber-Weiss cycle [25]. Interestingly, no DMPO-HO• signal was detected in SC Au NPs/RGO/H_2O_2 systems. Instead, a new characteristic triplet peak (1:1:1) corresponding to 2,2,6,6-tetramethyl-4-piperidinne-*N*-oxyl (TEMPO) appeared, indicating the generation of singlet oxygen ($^1O_2$) during the activation of H_2O_2 by SC Au NPs/RGO hybrids, while little $^1O_2$ single was detected over MT Au NPs/RGO/H_2O_2 systems (Fig. 5b). Meanwhile, slight $^1O_2$ and HO• signals were detected in Au NPs/H_2O_2 system due to the low catalytic activity of Au NPs alone, which is consistent with the observed R6G degradation experiments. These results indicate that SC Au NPs/RGO hybrids may induce a different catalytic pathway from the traditional Fenton-like catalytic reaction. $^1O_2$ may be the main reactive intermediate species in SC Au NPs/RGO/H_2O_2 system.

The role of ROS in the Fenton-like reaction was further verified by adding tert-butyl alcohol (TBA) and L-histidine (L-H) as radical scavengers of HO• and $^1O_2$ to quench R6G degradation process, respectively [26]. Fig. 5c presents an obvious decrease of the R6G degradation rates upon the addition of TBA and L-H into MT Au NPs/RGO/H_2O_2 system, indicating that both HO• and $^1O_2$ are involved in the degradation processes. On the contrary, TBA has little effect on R6G degradation in SC Au NPs/RGO/H_2O_2 system, while the degradation rate of R6G was significantly inhibited upon the addition of L-H (Fig. 5d). These results suggest that $^1O_2$ plays a dominant role in promoting R6G degradation in SC Au NPs/RGO/H_2O_2 system.

Based on the above results, a $^1O_2$ mediated pathway for organic pollutants degradation over SC Au NPs/RGO/H_2O_2 system is proposed, which is different from HO• pathway in traditional Fenton reaction. Generally, $^1O_2$ could generate in Fenton-like catalytic reaction *via* two possible pathways: the disproportionation of HO• and the oxidation of HO_2• [27]. No detectable signal of pivotal intermediate (HO•) indicates that the contribution of HO• to $^1O_2$ generation is very small. A more likely pathway is the oxidation of HO_2• to yield $^1O_2$. The first step involves that SC Au NPs on RGO surface may act as an electron relay (Au^{3+}/Au) to active H_2O_2 for HO_2• formation [8]. Subsequently, the homogeneous SC Au NPs on RGO sheet form uniform nanogaps between Au NPs, which induce a significant nanoconfinement effect and then facilitate $^1O_2$ generation [28].

In conclusion, a well crystalline SC Au NPs/RGO hybrid was fabricated by controllable growth of Au NPs on graphene sheet, which simultaneously possesses both unique Fenton-like catalytic activity to degrade organic pollutants and high SERS sensitivity to probe target molecules. The multifunction of SC Au NPs/RGO hybrid makes it an ideal platform for *in situ* SERS monitoring Fenton-like reaction. The proposed strategy would open new opportunities to design multifunctional platforms to achieve online environmental monitoring.

Declaration of competing interest

The authors declare that they have no known competing financial interests or personal relationships that could have appeared to influence the work reported in this paper.

Acknowledgments

This work was supported by the National Natural Science Foundation of China (Nos. 21577156, 21876184) and the Fundamental Research Funds for the Central University (No. 310421124).

Supplementary materials

Supplementary material associated with this article can be found, in the online version, at doi:10.1016/j.cclet.2021.07.051.

References

[1] E. Brillas, I. Sirés, M.A. Oturan, Chem. Rev. 109 (2009) 6570–6631.
[2] Z. Qiang, C. Liu, B. Dong, Y. Zhang, Chemosphere 78 (2010) 517–526.
[3] X. Wang, Y. Zhang, J. Hazard. Mater. 161 (2009) 202–207.
[4] M. Sun, G. Zhang, Y. Liu, et al., Chem. Eur. J. 21 (2015) 7611–7620.
[5] M.A. Voinov, J.O.S. Pagán, E. Morrison, et al., J. Am. Chem. Soc. 133 (2011) 35–41.
[6] X. Qian, M. Ren, Y. Zhu, et al., Environ. Sci. Technol. 51 (2017) 3993–4000.
[7] X.J. Yang, X.M. Xu, J. Xu, et al., J. Am. Chem. Soc. 135 (2013) 16058–16061.
[8] S. Navalon, R. Martin, M. Alvaro, et al., Angew. Chem. Int. Ed. 49 (2010) 8403–8407.
[9] L. Xu, J. Wang, Environ. Sci. Technol. 46 (2012) 10145–10153.
[10] J. Hu, X. Jing, L. Zhai, et al., Chemosphere 220 (2019) 77–85.
[11] Z.A. Nima, Y.R. Davletshin, F. Watanabe, et al., RSC Adv 7 (2017) 53164–53171.
[12] C. Wen, F. Liao, S. Liu, et al., Chem. Commun. 49 (2013) 3049–3051.
[13] M.M. Liang, Y.H. Wang, R. Shao, et al., Electrochem. Commun. 81 (2017) 38–42.
[14] R. Liu, H. Chen, L. Fang, et al., Environ. Sci. Technol. 52 (2018) 4244–4255.
[15] T.H. Yang, L.D. Huang, Y.W. Harn, et al., Small 9 (2013) 3169–3182.
[16] S. Yue, W. Ye, Z. Xu, Analyst 144 (2019) 5882–5889.
[17] W. Xie, B. Walkenfort, S. Schluecker, J. Am. Chem. Soc. 135 (2013) 1657–1660.
[18] S. Navalon, M. Miguel, R. Martin, et al., J. Am. Chem. Soc. 133 (2011) 2218–2226.
[19] L. Bian, Y. Liu, G. Zhu, et al., Ceram. Int. 44 (2018) 7580–7587.
[20] M. Liu, H. Zhao, S. Chen, et al., ACS Nano 6 (2012) 3142–3151.
[21] A. Parakh, S. Lee, M.T. Kiani, et al., Nano Lett. 20 (2020) 7767–7773.
[22] H. Zhang, S. Chen, X. Quan, et al., J. Mater. Chem. 21 (2011) 12986–12990.
[23] M. Turner, V.B. Golovko, O.P.H. Vaughan, et al., Nature 454 (2008) 981–983.
[24] P. Hildebrandt, M. Stockburger, J. Phys. Chem. 88 (1984) 5935–5944.
[25] W.H. Koppenol, Redox Rep. 6 (2001) 229–234.
[26] W. Liu, Y. Wang, Z. Ai, et al., ACS Appl. Mater. Interfaces 7 (2015) 28534–28544.
[27] S. Zhu, X. Li, J. Kang, et al., Environ. Sci. Technol. 53 (2019) 307–315.
[28] Z. Yang, J. Qian, A. Yu, et al., Proc. Natl. Acad. Sci. U. S. A. 116 (2019) 6659–6664.